

# Study of the EEC discrimination power on quark and gluon jet quenching effects in heavy-ion collisions at $\sqrt{s} = 5.02$ TeV

Shi-Yong Chen,<sup>1,2</sup> Zi-Xuan Xu,<sup>2</sup> Ke-Ming Shen,<sup>3</sup> Wei Dai\*,<sup>4</sup> Ben-Wei Zhang,<sup>2</sup> and Enke Wang<sup>5,2</sup>

<sup>1</sup>*Huanggang Normal University, Huanggang 438000, China*

<sup>2</sup>*Key Laboratory of Quark & Lepton Physics (MOE) and Institute of Particle Physics, Central China Normal University, Wuhan 430079, China*

<sup>3</sup>*East China University of Technology, Nanchang 330013, China*

<sup>4</sup>*School of Mathematics and Physics, China University of Geosciences, Wuhan 430074, China*

<sup>5</sup>*Guangdong Provincial Key Laboratory of Nuclear Science, Institute of Quantum Matter, South China Normal University, Guangzhou 510006, China*

(Dated: June 23, 2025)

We present a systematic investigation of flavor-dependent jet quenching using energy-energy correlators (EEC) in  $\sqrt{s} = 5.02$  TeV Pb+Pb collisions. Employing the improved SHELL model, which incorporates collisional and radiative energy loss, as well as medium response, we quantify distinct quenching signatures for quark and gluon jets. Key findings include: (1) Pure quark jets exhibit strong EEC enhancement at large angular scales, while gluon jets show a bimodal enhancement pattern at both small and large scales; (2) Dual-shift decomposition in the EEC ratio reveals shifts toward large primarily driven by energy loss, while small- $R_L$  shifts extend beyond selection bias and indicate intrinsic enhancement of the gluon-initiated jets; (3) Quark jets experience global suppression of averaged energy weight  $\langle \text{weight} \rangle(R_L)$ , whereas gluon jets exhibit concentration toward small  $R_L$ ; (4) Mechanism decomposition identifies elastic energy loss concentrating  $\langle \text{weight} \rangle(R_L)$  toward small  $R_L$ , radiative loss dominating quark jet modification, and medium response amplifying large  $R_L$  enhancement via soft hadrons. The observed flavor dependence in EEC modifications is dominantly driven by intrinsic jet structure differences rather than medium-induced mechanisms. We propose photon-tagged jets as quark proxies and inclusive charged-hadron jets as gluon proxies, finding they reproduce the respective flavor-specific quenching patterns. Our work establishes the EEC as a precision probe of color-charge-dependent jet-medium interactions, providing new constraints for the detailed  $\hat{q}$  extraction and QGP tomography, while highlighting the critical role of pre-quenching flavor asymmetries.

PACS numbers: 13.87.-a; 12.38.Mh; 25.75.-q

## I. INTRODUCTION

The creation of a deconfined quark-gluon plasma (QGP) in relativistic heavy-ion collisions provides a unique opportunity to study quantum chromodynamics (QCD) under extreme conditions in the laboratory [1–5]. Highly energetic jets-collimated sprays of particles resulting from the fragmentation of hard-scattered partons produced in the initial collisions, served as precision probes to the novel properties of this QCD medium. The phenomenon of jet quenching, characterized by the significant suppression of high-transverse momentum ( $p_T$ ) hadrons and jets relative to scaled proton-proton collisions, arises primarily from parton energy loss mechanisms, such as medium-induced gluon radiation and elastic collisions [6–8]. Quantifying this energy loss provides critical, direct insights into the QGP's transport coefficients. To dissect the complex space-time evolution of the in-medium parton shower and differentiate between competing energy loss mechanisms, jet substructure observables have emerged as indispensable, high-resolution tools [9–35]. These observables quantify the modification of the jet's internal energy flow and fragmentation

pattern caused by interactions with the QGP. Recent significant advances include detailed measurements of differential jet shapes [26, 27, 36–38], fragmentation functions [39–42], groomed jet observables [21, 43], collectively offering a multi-dimensional tomography of jet-medium interactions.

Among jet substructure observables, the energy-energy correlator (EEC) [44–47] is particularly significant due to its sensitivity to soft and collinear radiation patterns within jets. Defined as the energy-weighted angular correlation between particle pairs, the EEC probes jet internal structure in elementary collisions and has emerged as a powerful tool for studying QCD dynamics [48–74]. In heavy-ion collisions, it elucidates the onset of color coherence in medium-induced splittings [75–82], reveals the medium response effect, mass hierarchy in heavy-flavor jets [83–86], and exposes cold nuclear matter effects in small systems [87–89]. The impact of selection bias on the modification of the EEC is also discussed in [90, 91]. Moreover, EEC has also garnered significant attention among experimentalists [92–95], with STAR, CMS, and ALICE collaborations conducting dedicated measurements of this observable in heavy-ion collisions.

Flavor-dependent parton energy loss is a fundamental aspect governing jet evolution within the QGP [7, 96]. Distinct Casimir color factors not only lead to differences in the magnitude of energy loss between quarks and glu-

\*weidai@mail.cug.edu.cn

ons but also subject them to differential in-medium splitting [97–100]. This inherent difference in energy loss rates manifests directly as distinct medium modifications in jet substructure observables, such as jet charge [29, 101, 102] and jet shape [32, 36, 37, 103]. However, the in-medium radiation pattern of this quark/gluon difference on jet substructure observable in heavy-ion collisions remains lacking in studies. Therefore, it is compelling to investigate the flavor-dependent jet quenching pattern within the finer in-jet substructure using the EEC.

The remainder of the paper is organized as follows. In Sec. II, we introduce the definition of the EEC used for the ALICE experimental study, and the p+p baseline of the EEC distributions for inclusive jets in three different jet transverse momentum intervals will be calculated to confront the experimental data. In Sec. III we calculate and compare the EEC distributions for inclusive jets in Pb+Pb and p+p at  $\sqrt{s} = 5.02$  TeV for the transverse momentum interval 40 – 60 GeV, to de-

rive the medium modification ratios (A+A/p+p). The in-depth phenomenology exploration of such an observable is also presented and helps us discuss the differences in the jet quenching of quark- and gluon-initiated jets from the following four aspects: their respective Energy-Energy Correlation (EEC) distributions, the impacts of different jet quenching mechanisms on them respectively, the different modifications of the fine structures revealed by the intra-jet EEC, and their different selection bias effects. Finally, we close this paper to a summary in Sec. IV.

## II. EEC DISTRIBUTIONS IN P+P COLLISIONS

The ALICE defined EEC describes the energy-weighted cross-section of particle pairs as functions of the angular distance between each pair as follows [95]:

$$\Sigma_{\text{EEC}}(R_L) = \frac{1}{N_{\text{jet}} \cdot \Delta R} \int_{R_L - \frac{1}{2}\Delta R}^{R_L + \frac{1}{2}\Delta R} \sum_{\text{jets}} \sum_{i,j} \frac{p_{T,i} p_{T,j}}{p_{T,\text{jet}}^2} \delta(R'_L - R_{L,ij}) dR'_L. \quad (1)$$

where all final state particle pairs  $(i, j)$  inside each jet are summed up. The angular distance between each pair is defined in the  $\eta - \varphi$  plane as  $R_{L,ij} = \sqrt{(\varphi_j - \varphi_i)^2 + (\eta_j - \eta_i)^2}$ , which  $\Delta R$  is the angular bin width and  $N_{\text{jet}}$  is the total number of jets. Then we noticed it is a distribution observable defined in a jet.

We start by calculating the defined EEC distributions of inclusive jets in p+p collisions to provide a baseline for further studies. In this work, we use a Monte Carlo (MC) event generator PYTHIA v8.309 [104] with Monash 2013 tune [105] to simulate jet productions in p+p collisions. To confront our calculated results with experimental data, we use the same kinematic cuts of events as adopted by the ALICE measurements [94]. All jets are reconstructed by the anti- $k_T$  algorithm with radius parameter  $R = 0.4$  from charged particles with  $p_T \geq 1$  GeV using the FASTJET v3.4.0 package [106]. These reconstructed jets are accepted in the transverse momentum range  $20 \text{ GeV} < p_{T,\text{jet}} < 80 \text{ GeV}$  and rapidity range of  $|\eta_{\text{jet}}| < 0.5$ . Our numerical results of  $\Sigma_{\text{EEC}}$  as functions of  $R_L$  for inclusive charged jets and their comparisons with ALICE data in p+p collisions at  $\sqrt{s} = 5.02$  TeV are shown in Fig. 1.

We can observe that our numerical results show fairly good agreement with experimental measurements in p+p collisions in the three  $p_T$  intervals, which will serve as input and baseline for the subsequent study in Pb+Pb collisions. The EEC distributions are shifted to a lower  $R_L$  region with the increasing jet  $p_T$ . We can conclude that, with the increment of jet  $p_T$ , the EEC distributions shift to smaller  $R_L$ , and the height of the distribution will

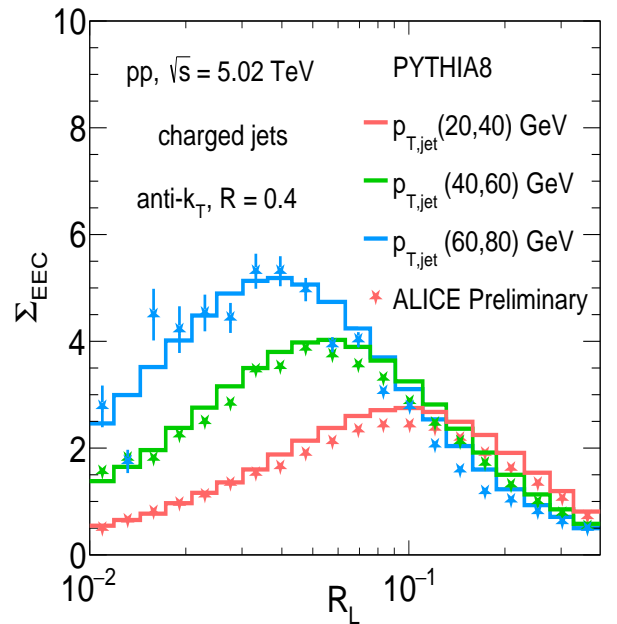


FIG. 1: PYTHIA8 simulation results of defined  $\Sigma_{\text{EEC}}$  distributions as functions of  $R_L$  for inclusive charged jets with a jet size of  $R = 0.4$  in three jet transverse momentum intervals:  $20 \text{ GeV} < p_{T,\text{jet}} < 40 \text{ GeV}$ ,  $40 \text{ GeV} < p_{T,\text{jet}} < 60 \text{ GeV}$  and  $60 \text{ GeV} < p_{T,\text{jet}} < 80 \text{ GeV}$  produced in p + p collisions at  $\sqrt{s} = 5.02$  TeV. The results are compared with the ALICE experimental data [94].

increase which is surely affected by the different number of particle pairs within one jet in each  $p_T$  interval. To extract such an effect, it is natural to divide the EEC observable into two major parts rewritten as:

$$\Sigma_{\text{EEC}}(R_L) = \frac{N_{\text{pair}}^{\text{total}}}{N_{\text{jet}}} \cdot \frac{\Delta N_{\text{pair}}}{N_{\text{pair}}^{\text{total}} \Delta R}(R_L) \cdot \langle \text{weight} \rangle(R_L) \quad (2)$$

where we average the energy weight term,  $p_{T,i} p_{T,j} / p_{T,\text{jet}}^2$ , to every particle pair within every jet in each angular bin  $\Delta R$ , denoted as  $\langle \text{weight} \rangle$ , therefore we can simply replace the integration and then sum over jets and  $i, j$  into a summed number of pairs within each bin  $\Delta R$ , denoted as  $\Delta N_{\text{pair}}$ . Consequently, Eq. 2 appears as: the averaged number of particles within a jet, normalized  $R_L$  distribution on the number of pairs, and the averaged energy weight distribution as a function of  $R_L$ . It will benefit further explorations and discussions.

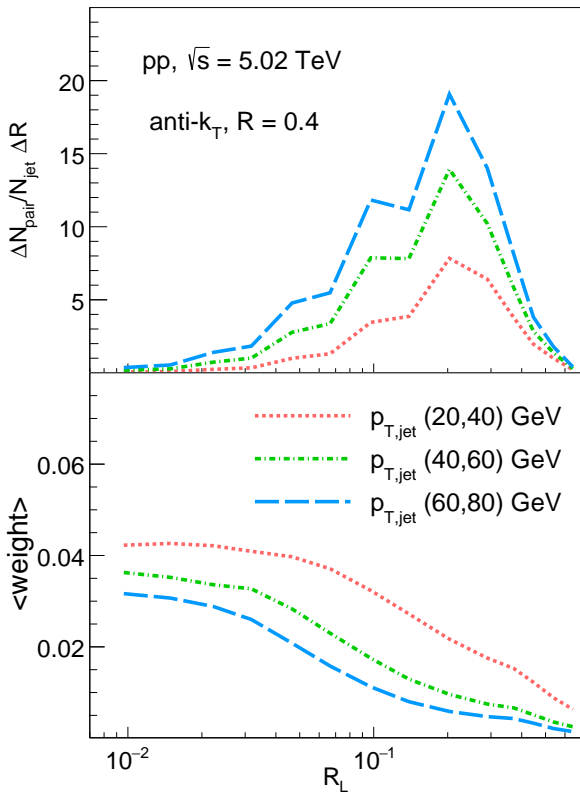


FIG. 2: Number of jets normalized pair-number distributions (upper panel) and averaged energy weight (lower panel) distributions as functions of  $R_L$  for inclusive charged jets in three jet transverse momentum intervals:  $20 \text{ GeV} < p_{T,\text{jet}} < 40 \text{ GeV}$ ,  $40 \text{ GeV} < p_{T,\text{jet}} < 60 \text{ GeV}$  and  $60 \text{ GeV} < p_{T,\text{jet}} < 80 \text{ GeV}$  produced in p + p collisions at  $\sqrt{s} = 5.02 \text{ TeV}$ .

We plot the  $R_L$  distributions of the total number of pairs normalized to every inclusive charged jet produced in p + p collisions at  $\sqrt{s} = 5.02 \text{ TeV}$  for all three  $p_{T,\text{jet}}$  intervals in the upper panel of Fig. 2, denoted as the

product of the first two terms in Eq. 2. The corresponding  $R_L$  distributions of the averaged weight  $\langle \text{weight} \rangle$  are also demonstrated in the bottom panel of Fig. 2.

We find in the upper panel that most of the particle-pairs are distributed around  $R_L = 0.2$ , and there is no jet transverse momentum dependence of the peak position. The distribution height increases with the enhancement of  $p_{T,\text{jet}}$  because the number of constituents within the jets increases as a consequence. In the bottom panel, the role of the  $\langle \text{weight} \rangle$  is to shift the distribution of particle pairs toward smaller  $R_L$  directions, while the heights of the  $\langle \text{weight} \rangle$  distribution are also determined by the jet transverse momentum. Higher jet transverse momentum leads to more constituent particles within the jet, consequently resulting in lower  $\langle \text{weight} \rangle$  values.

### III. EEC DISTRIBUTIONS IN A+A COLLISIONS

#### A. Improved SHELL model

In relativistic heavy-ion collisions, partons produced from initial hard scatterings undergo energy loss through interactions with the QGP. To simulate this process, we employ the improved SHELL model—a Monte Carlo framework that concurrently handles both elastic, inelastic scattering processes and the medium response during jet propagation. The SHELL model has been quantitatively validated against multiple experimental observables, establishing its reliability for jet quenching studies [32, 107–111]. The model initializes parton positions via sampling from a Glauber-model-based nuclear geometry [112], then they will transport through the QGP step-by-step. The radiative energy loss mechanism is implemented through a stochastic implementation approach. The probability of a gluon radiation when traversing through the QGP medium during each time step  $\Delta t$  can be expressed as:

$$P_{\text{rad}}(t, \Delta t) = 1 - e^{-\langle N(t, \Delta t) \rangle}. \quad (3)$$

Here  $\langle N(t, \Delta t) \rangle$  is the averaged number of radiated gluons, which can be calculated from the medium induced radiated gluon spectrum within the Higher-Twist (HT) method[113–116]:

$$\frac{dN}{dx dk_{\perp}^2 dt} = \frac{2\alpha_s C_s P(x) \hat{q}}{\pi k_{\perp}^4} \sin^2\left(\frac{t - t_i}{2\tau_f}\right) \left(\frac{k_{\perp}^2}{k_{\perp}^2 + x^2 M^2}\right)^4 \quad (4)$$

where  $\alpha_s$  is the strong coupling constant,  $x$  and  $k_{\perp}$  denote the energy fraction and the  $p_T$  of the radiated gluon,  $M$  is the mass of the parent parton. Only the gluon with a lower  $x_{\text{min}} = \mu_D/E$  cut-off is allowed to emit, and  $\mu_D$  is the Debye screening mass.  $P(x)$  is the QCD splitting function in vacuum,  $C_s$  denotes the Casimir factor for gluon ( $C_A$ ) and quark ( $C_F$ ).  $\tau_f = 2Ex(1-x)/(k_{\perp}^2 + x^2 M^2)$  is the formation time of the radiated gluons.  $\hat{q} = q_0(T/T_0)^3 p_{\mu} u^{\mu}$  is the jet transport parameter, where  $q_0 = 1.5 \text{ GeV}^2/\text{fm}$ ,  $u^{\mu}$  is the local

velocity of the QGP, and  $T_0$  is the initial temperature. The jet transport parameter is used to control the magnitude of energy loss due to jet-medium interaction. The number of radiated gluons is sampled from a Poisson distribution during each inelastic scattering.

$$P(n_g, t, \Delta t) = \frac{\langle N(t, \Delta t) \rangle^{n_g}}{n_g!} e^{-\langle N(t, \Delta t) \rangle} \quad (5)$$

In our calculation,  $P_{rad}(t, \Delta t)$  would first be evaluated to determine whether the radiation happens during  $\Delta t$ . If accepted, the Poisson distribution  $P(n_g, t, \Delta t)$  is used to sample the number of radiated gluons. At last, the energy fraction ( $x$ ) and transverse momentum ( $k_\perp$ ) of the radiated gluon could be sampled based on the spectrum shown in Eq. 4.

To calculate the collisional energy loss of these showered partons, a Hard Thermal Loop (HTL) formula[117] has been adopted in this work:  $\frac{dE^{coll}}{dt} = \frac{\alpha_s C_s \mu_D^2}{2} \ln \frac{\sqrt{ET}}{\mu_D}$ . The space-time evolution of the expanding fireball is given by the CLVisc hydrodynamic model[118]. When local temperature falls below  $T_c = 165$  MeV, all the showered partons stop their propagation in the QGP medium and fragment into hadrons. In this work, we first construct strings using the colorless method developed by the JETSCAPE collaboration [119], then perform hadronization and hadron decays using the PYTHIA Lund string method.

We also include the medium response effect in the calculation by considering that the lost energy in the collisional process is deposited into the evolved QGP medium. This deposited energy disturbs the medium, exciting a hydrodynamic wake correlated with the parton's direction. Following freeze-out, this wake hadronizes, producing soft hadrons that can be reconstructed within the jet cone. To incorporate this medium response effect, we employ a hybrid approach based on the Cooper-Frye freeze-out prescription with perturbations [39, 120]. The resulting distribution of wake particles is given by:

$$E \frac{d\Delta N}{d^3p} = \frac{1}{32\pi} \frac{m_T}{T^5} \cosh(y - y_j) \exp \left[ -\frac{m_T}{T} \cosh(y - y_j) \right] \times \left\{ p_T \Delta P_T \cos(\phi - \phi_j) + \frac{1}{3} m_T \Delta M_T \cosh(y - y_j) \right\}, \quad (6)$$

Here,  $m_T$ ,  $p_T$ ,  $y$ , and  $\phi$  denote the transverse mass, transverse momentum, rapidity, and azimuthal angle of the emitted wake hadrons, respectively. The variables  $y_j$  and  $\phi_j$  represent the rapidity and azimuthal angle of the initiating energetic parton.  $T$  denotes the freeze-out temperature of the hot QCD medium.  $\Delta M_T = \Delta E / \cosh(y_j)$  and  $\Delta P_T$  are the transverse mass and transverse momentum transferred from the jet to the medium, where  $\Delta E$  is the deposited energy.

## B. Collisional vs. Radiative vs. Medium Response

The angular distribution of the EEC within a jet inherently reflects medium-induced modifications of jet constituents, offering a direct connection to the scale and structure of the QGP. This distribution can be used to study jet-induced medium response, medium-induced radiation, and transverse momentum broadening. We calculate the  $\Sigma_{EEC}$  distributions as functions of  $R_L$  for inclusive charged jets in Pb+Pb collisions at  $\sqrt{s} = 5.02$  TeV to predict the possible ALICE measurement. We demonstrate in Fig. 3 the A+A/p+p ratio of the  $\Sigma_{EEC}$  distributions as functions of  $R_L$  with the jet radius of  $R = 0.4$  in the jet  $p_T$  interval of 40 – 60 GeV shown in the solid blue line. We find clear enhancements at  $R_L > 0.3$  and  $R_L < 0.06$ , as well as suppression at  $R_L$  around 0.06 – 0.3. From the distribution shifting point of view, it implies there are shifts toward larger  $R_L$  and smaller  $R_L$  at the same time. There have to be two effects competing with each other. To isolate the contributions and effects from different jet quenching mechanisms, we also plot in the same figure the A+A/p+p ratios as functions of  $R_L$ : only considering radiative energy loss, denoted as the dashed dotted line; only considering collisional energy loss, denoted as the dotted line; considering both collisional and radiative energy loss but excluding medium response effect, denoted as the dashed line. We will apply the same notation in the following discussion.

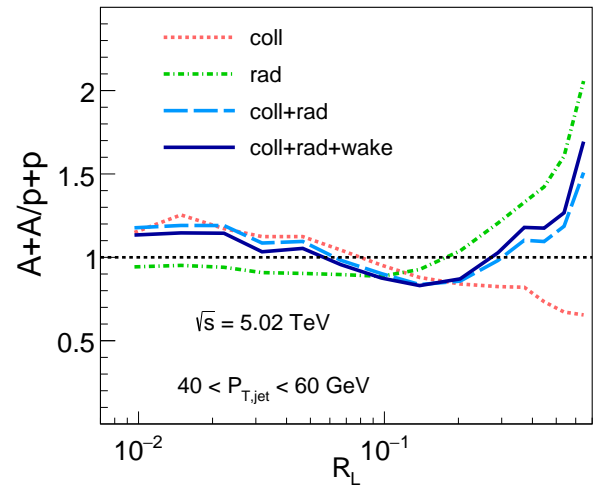


FIG. 3: A+A/p+p ratios of the  $\Sigma_{EEC}$  distributions as functions of  $R_L$  for inclusive charged jets with a radius of  $R = 0.4$  in central (0 – 10%) Pb + Pb collisions at  $\sqrt{s} = 5.02$  TeV in jet  $p_T$  interval 40 – 60 GeV calculated considering 4 scenarios of jet quenching mechanism: collisional energy loss only, radiative energy loss only, collisional+radiative energy loss and collisional+radiative energy loss+medium response.

Firstly, we find that the pure collisional energy loss process leads to a gradual enhancement in the smaller  $R_L$  region and a gradual suppression in the larger  $R_L$  region,

indicating that the energy loss mechanism, which does not alter the particle propagation direction, results in a concentration of the energy weight distribution toward smaller  $R_L$  values. Secondly, the pure radiative energy loss process leads to a rapid enhancement with increasing  $R_L$  in  $R_L > 0.2$  and a slight suppression at  $R_L < 0.2$ , indicating a clear broadening effect toward larger  $R_L$  values in the distribution. It is a typical consequence of the medium-induced gluon radiation. The final A+A/p+p ratio is almost exactly the result of the competition of the two mechanisms. The medium response effect seems visible and mild in this specific observable, but it has the same diffusion behaviour of enhancing the distribution in the larger  $R_L$  values and suppressing that in the smaller  $R_L$  region as the radiative energy loss process.

To gain deeper insight into the physical implications of this result, we examine the theoretical predictions from three perspectives: probing finer jet substructures revealed by the EEC observable itself, specifically the distribution of average paired-energy weight versus  $R_L$  shown in Fig. 2; impact of selection bias, which is a common effect in jet substructure observables, on the EEC measurements; capability of this observable to distinguish quark-initiated jets from gluon-initiated jets in jet quenching, along with the underlying mechanisms for such differences.

### C. In-jet finer substructure as revealed by the EEC

Applying the strategy discussed in Eq. 2 and Fig. 2, we firstly calculate the ratio of the  $R_L$ -distribution of paired-particle counts normalized to the number of jets in Pb + Pb collisions to that in p + p collisions shown in the upper panel of Fig. 4. Elastic energy loss leads to a reduction in the  $R_L$ -distribution of paired-energy counts in A+A compared to the p+p case, and this reduction becomes more pronounced with increasing  $R_L$ . The overall suppression demonstrates a reduction in the number of particle pairs. The slope of the curve indicates that it leads to an enhancement of the distribution in the small  $R_L$  region relative to that in the large  $R_L$  region. The dashed-dotted line demonstrates that radiative energy loss causes the  $R_L$ -distribution of paired-energy counts for jets in A+A collisions to shift towards larger  $R_L$ . The dashed line shows how the two mechanisms compete with each other. The comparison between the total effect represented by the solid line and the dashed line reveals that the effect of medium response on the  $R_L$ -distribution of paired-particle counts is manifested as an enhancement in the large  $R_L$  region. Furthermore, the medium response resulting in an increase in the number of jet constituents contributes entirely to the distribution in this specific region.

From the bottom panel of Fig. 4, we observe that all types of jet quenching mechanisms lead to an elevation of the averaged energy-energy weights ( $\langle \text{weight} \rangle$ s) in the small  $R_L$  region relative to those in the large  $R_L$  region. This behavior explains why the A+A/p+p ratio of the

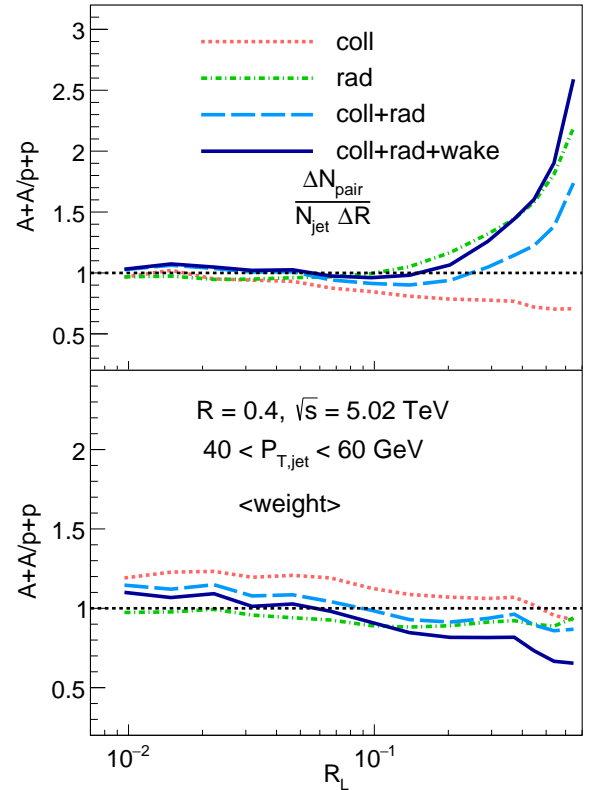


FIG. 4: Ratio of the  $R_L$  distribution of paired-particle counts normalized to the number of jets in Pb + Pb collisions to that in p + p collisions (upper panel) and the ratio the  $R_L$ -distribution of averaged energy-energy weight in Pb + Pb collisions to that in p + p collisions (lower panel) for inclusive charged jets with the size of  $R = 0.4$  in the jet transverse momentum interval of  $40 \text{ GeV} < p_{T,\text{jet}} < 60 \text{ GeV}$  produced at  $\sqrt{s} = 5.02 \text{ TeV}$ . The results of the four jet quenching scenarios are also plotted same way as in Fig. 3.

EEC shown in Fig. 3 exhibits an enhancement in the small  $R_L$  region, while its rise, when moving towards the large  $R_L$  region, is weaker than that observed in the paired-particle count distribution in the upper panel. The ratio value obtained from radiative energy loss is lower than that from collisional energy loss because radiative energy loss increases the number of particle pairs, whereas collisional energy loss reduces it. The inclusion of the medium response effect, due to the resulting increase in the number of jet constituents, causes a reduction in the  $\langle \text{weight} \rangle$ s. This creates a stark contrast to the sharp rise it induces in the paired-particle count distribution within the large  $R_L$  region, leading to a mild overall effect of the medium response to the A+A/p+p ratio of EEC. Therefore, we find that the upper and lower parts shown in the figure exhibit exactly opposite trends in their response to changes in the number of jet constituents, resulting in a partial cancellation effect.



### D. Quark-initiated jets versus gluon-initiated jets

Still, we need to examine the reason why the  $\langle \text{weight} \rangle$  distribution in A+A collisions is relatively more concentrated towards the small  $R_L$  region. As suggested by the jet- $p_T$  dependence of the EEC distribution shown in Fig. 1, this phenomenon may be attributed to selection bias. But does this imply that energy loss mechanisms cannot drive the  $\langle \text{weight} \rangle$  towards larger  $R_L$  angles? Is this phenomenon consistent for both quark- and gluon-initiated jets? We find that a comprehensive understanding of flavor-dependent jet-quenching effects on the EEC observable remains elusive. To address this, we intend to conduct further discussion focusing on the following aspects: initial p+p production, different jet quenching mechanisms, in-jet finer substructure as revealed by the EEC, selection bias effect, and flavor-dependent attribution. We begin our discussion by comparing purely quark-initiated jets and purely gluon-initiated jets generated by PYTHIA.

**initial p+p production** - Given the experimental challenge of identifying or defining quark versus gluon-initiated jets, we adopt a simulation-based approach. Using PYTHIA 8, we generate events from hard processes constrained to produce exclusively quarks or exclusively gluons. Jets are then reconstructed in these events and used for our case study.

In Fig. 5 we plot  $\Sigma_{\text{EEC}}$  distributions as functions of  $R_L$  for inclusive charged jets, pure gluon-initiated and quark-initiated jets with a size of  $R = 0.4$  in the jet transverse momentum interval of  $40 \text{ GeV} < p_{T,\text{jet}} < 60 \text{ GeV}$  produced in p+p collisions at  $\sqrt{s} = 5.02 \text{ TeV}$  simultaneously. We observe that gluon-initiated jets peak around  $R_L = 0.08$ , while quark-initiated jets exhibit higher distribution values and are more concentrated in the small- $R_L$  region. Inclusive charged jets represent a mixture of the two, and their distribution closely resembles that of gluon-initiated jets. This observation also reveals that within this kinematic regime, the charged-hadron jet sample is predominantly dominated by gluon-initiated jets. The transition from gluon-initiated to quark-initiated jets produces an effect similar to what is achieved by increasing the jet  $p_T$ .

**different jet quenching mechanism** - In Fig. 6, within the same kinematic regime, the jet quenching patterns for different flavor-initiated jets are investigated individually. First of all, we present the A+A/p+p ratios of the  $\Sigma_{\text{EEC}}$  distributions for quark-initiated jets and gluon-initiated jets in the upper and lower panels, respectively. Below  $R_L = 0.15$ , a slight and gradual suppression is observed for quark-initiated jets in the upper panel, while beyond  $R_L = 0.15$ , the ratio exhibits an increasing behavior with rising  $R_L$ . The enhancement observed in the large- $R_L$  region reveals a distinct diffusion effect induced by jet quenching for quark-initiated jets. However, the suppression seen in the small- $R_L$  region indicates that the selection bias effect is not manifested. In the lower panel, we observe a significant enhancement for gluon-initiated jets in the small- $R_L$  region below 0.07. This enhancement becomes more pronounced as the  $R_L$  decreases. Addition-

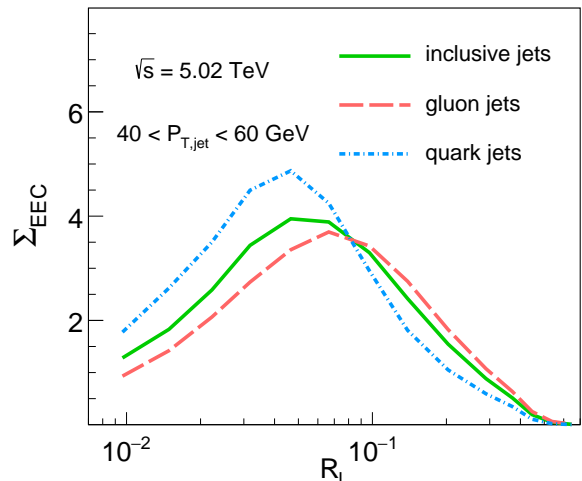


FIG. 5: PYTHIA8 simulation results of defined  $\Sigma_{\text{EEC}}$  distributions as functions of  $R_L$  for inclusive charged jets, pure gluon-initiated jets and quark-initiated jets with a jet size of  $R = 0.4$  in the jet transverse momentum interval of  $40 \text{ GeV} < p_{T,\text{jet}} < 60 \text{ GeV}$  produced in p + p collisions at  $\sqrt{s} = 5.02 \text{ TeV}$ .

ally, a substantial increase is also seen in the large- $R_L$  region beyond 0.4, where the ratio rises monotonically with increasing  $R_L$ .

Fig. 1 indicates that jets with higher transverse momentum tend to populate the distribution in smaller- $R_L$  region. The enhancement observed in the small- $R_L$  region of this figure likely originates from contributions of higher- $p_T$  jets before significant energy loss occurs. Notably, quark- and gluon-initiated jets exhibit markedly distinct responses to this mechanism. This difference may partly be explained by examining Fig. 5: quark-initiated jets predominantly distribute in intrinsically smaller  $R_L$  regions, whereas gluon-initiated jets favor larger  $R_L$  regions. Furthermore, in the large- $R_L$  region, the observed enhancement is smaller for gluon jets than for quark jets. These characteristic differences collectively constitute the discriminatory power of the EEC observable in distinguishing the jet quenching signatures of quark-initiated versus gluon-initiated jets.

Simultaneously, we also computed the isolated impact of different jet quenching mechanisms on their respective A+A/p+p ratios, shown alongside the curve representing the overall consideration of the jet quenching mechanisms, following the methodology employed in Fig. 3. For the pure elastic energy loss mechanism, we find that regardless of whether for gluon-initiated or quark-initiated jets, it consistently leads to enhancement in the small- $R_L$  region and suppression in the large- $R_L$  region. This tends to increase their relative weighting at small  $R_L$ . However, the effect is less pronounced for quark-initiated jets compared to gluon-initiated jets, noting that initially, quark jets already exhibit a stronger tendency to

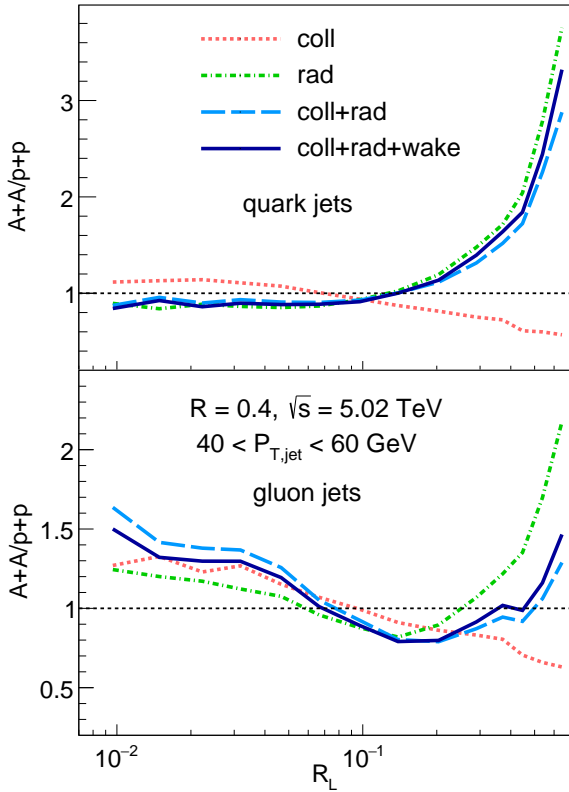


FIG. 6:  $A+A/p+p$  ratios of the  $\Sigma_{EEC}$  distributions for quark-initiated jets (upper panel) and gluon-initiated jets (bottom panel) separately calculated in the four jet quenching scenarios plotted in the same manner and the same kinetic region as in Fig. 3.

populate the small- $R_L$  region than gluon jets. In contrast, the radiative energy loss mechanism exhibits significantly greater differences between quark-jets and gluon-jets than elastic energy loss. For quark-initiated jets, radiative energy loss manifests as suppression in the small- $R_L$  region and enhancement in the large- $R_L$  region. Its behavior almost entirely dictates the overall  $A+A/p+p$  ratio pattern, rendering the contribution from elastic energy loss negligible. The medium response effect provides only a minor enhancing contribution in the large  $R_L$  region. For gluon-initiated jets, radiative energy loss manifests as an enhancement in both the small and large  $R_L$  regions. Overall, radiative energy loss still dominates the  $A+A/p+p$  ratio for gluon jets. However, its dominance is more substantially diminished by the opposing effects of elastic energy loss compared to the case in quark-initiated jets, where it holds a stronger position.

**selection bias effect** - Through the above analysis and comparisons, we recognize the critical need to further characterize the selection bias effects experienced separately by quark- and gluon-initiated jets, moving beyond intuitive interpretations based solely on the  $p_T$ -dependence observed in Fig. 1. We employ the following methodology: Jets with reconstructed transverse mo-

mentum in the 40 – 60 GeV range in  $A+A$  collisions are categorized into two classes: *Falldown*, jets originating from partons that, prior to energy loss, would have produced jets with  $p_T > 60$  GeV in the corresponding  $p+p$  collisions. *Survival*, jets originating from partons that, before energy loss, would have produced jets with  $p_T$  in the 40 – 60 GeV range in the corresponding  $p+p$  collisions. In Fig. 7, we comparatively present the  $A+A/p+p$  ratios of the EEC distributions for both quark-initiated and gluon-initiated jets, separately showing the contributions originating from the *Falldown* and *Survival* components for each flavor.

We find that the energy loss patterns manifested by the *Falldown* and *Survival* components are dynamically analogous. The characteristic differences in energy loss signatures fundamentally originate from the flavor of the initial partons. Comparatively, the *Falldown* contribution consistently exhibits a stronger enhancing effect in the small- $R_L$  region while producing relatively weaker diffusion in the large- $R_L$  region. The combined effect observed in Fig. 3 arises from the mixture of these *Falldown* and *Survival* components. Examining the *Survival* component in isolation reveals that in the small- $R_L$  region, even without the amplified selection bias effect intrinsic to the *Falldown* population, gluon-initiated jets inherently generate a slight enhancement due to their characteristic energy loss pattern. The selection bias effect further augments this enhancement. Simultaneously, we note that the enhancing effect of selection bias in this region remains insufficient to counteract the suppressing effect of quark jet energy loss. This leads to the empirical observation that gluon jets appear more susceptible to selection bias. The underlying physics, however, indicates that both quark and gluon jets experience selection bias. The observed difference primarily arises from the flavor-dependent characteristics of energy loss imprinted on the EEC observable.

**in-jet finer substructure of EEC** - To gain further insight into the aforementioned differences in jet quenching effects between quark- and gluon-initiated jets through the substructure details revealed by the EEC, we present the following in Fig. 8. Upper panels: the  $A+A/p+p$  ratios of the normalized paired-particle count  $R_L$  distributions (normalized per jet) for quark-initiated jets (left) and gluon-initiated jets (right). Lower panels: the  $A+A/p+p$  ratios of the  $\langle \text{weight} \rangle$   $R_L$  distributions for quark-initiated jets (left) and gluon-initiated jets (right). Additionally, results showing the isolated effects of different jet quenching mechanisms are overlaid in each panel.

Let's begin with the  $A+A/p+p$  ratios of the normalized paired-particle count  $R_L$  distributions. For quark-initiated jets: The angular distribution of paired particles diffuses toward larger  $R_L$  values. Elastic energy loss suppresses this trend by inducing suppression at large  $R_L$ , but the medium response effect compensates for this suppression. Consequently, the net effect nearly matches that of radiative energy loss. For gluon-initiated jets: The physical behavior pattern is analogous, although the diffusion toward larger  $R_L$  occurs to a lesser extent than

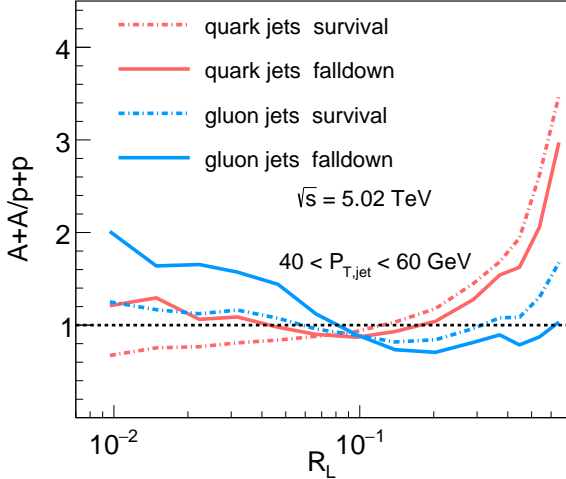


FIG. 7:  $A+A/p+p$  ratios for EEC distributions as a function of  $R_L$  for quark- and gluon-initiated jets with two categories: *Survival* and *Falldown* in central ( $0-10\%$ ) Pb+Pb collisions at  $\sqrt{s} = 5.02$  TeV in jet  $p_T$  interval  $40-60$  GeV.

in quark jets.

Turning now to the  $A+A/p+p$  ratios of the  $\langle \text{weight} \rangle$   $R_L$  distributions: for quark-initiated jets, modifications to the  $\langle \text{weight} \rangle$  are relatively mild overall. A slight enhancement only begins to emerge beyond  $R_L = 0.3$ . Furthermore, the entire modification remains dominated by radiative energy loss, even though the elastic energy loss mechanism exhibits opposing behavior, consistent with the indication from the upper panel. Similarly, we observe that the medium response effect provides a significant suppressing contribution in the large- $R_L$  region, directly counteracting the enhancement induced by radiative energy loss. Consequently, this results in an overall gentle modification, suggesting that the  $\langle \text{weight} \rangle$  distribution experiences no significant shift across the entire  $R_L$  range. For gluon-initiated jets, the shift of the  $\langle \text{weight} \rangle$  towards concentration in the small- $R_L$  region is markedly pronounced. Both radiative and elastic energy loss contribute in the same direction (towards this shift), and the medium response effect further suppresses the distribution in the large- $R_L$  region.

Building on the two refined aspects of jet substructure quenching effects, we now analyze the results in Fig. 6, which reflect their combined impact. For quark-initiated jets, elastic energy loss contributes negligibly. Both radiative energy loss and medium response increase the number of jet constituents. This significantly enhances the paired-particle count  $R_L$  distribution while substantially suppressing the  $\langle \text{weight} \rangle$ . In the small- $R_L$  region, minimal modification to paired-particle counts dominates. The suppression of  $\langle \text{weight} \rangle$  thus causes an overall suppression in the total EEC  $A+A/p+p$  ratio. In the large- $R_L$  region, the strong enhancement in paired-particle counts is partially counteracted by suppressed

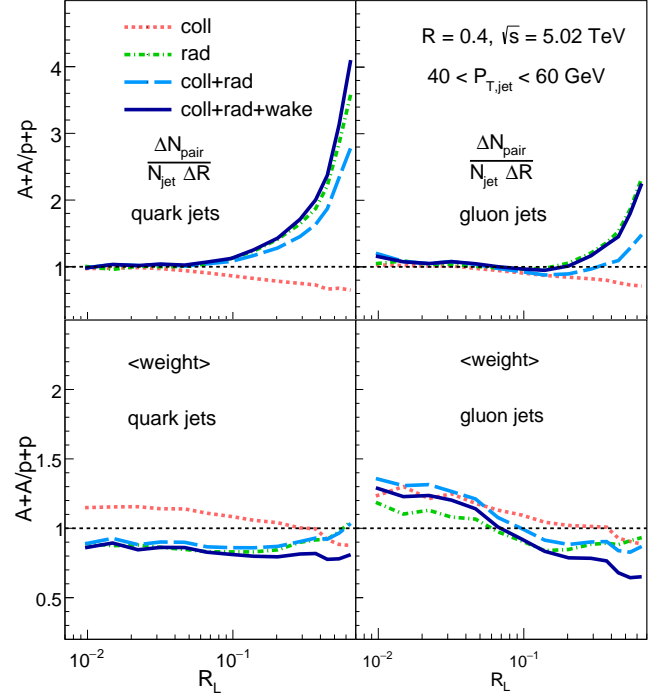


FIG. 8: The  $A+A/p+p$  ratios of the number of jets normalized paired-particle count  $R_L$  distributions for quark-initiated jets (left) and gluon-initiated jets (right) are plotted in the upper panels; The  $A+A/p+p$  ratios of the  $\langle \text{weight} \rangle$   $R_L$  distributions for quark-initiated jets (left) and gluon-initiated jets (right) are plotted in the lower panels. The jets are with a jet size of  $R = 0.4$  in the jet transverse momentum interval of  $40 \text{ GeV} < p_{T,\text{jet}} < 60 \text{ GeV}$  produced in Pb + Pb collisions at  $\sqrt{s} = 5.02$  TeV.

$\langle \text{weight} \rangle$ . Nevertheless, a significant net enhancement persists. For gluon-initiated jets, the enhancement in the paired-particle count  $R_L$  distribution is weaker than in quark jets. The critical difference lies in modifications to the  $\langle \text{weight} \rangle$   $R_L$  distribution: in the small  $R_L$  region, an enhancement is observed; in the large  $R_L$  region, pronounced suppression is observed. Consequently, enhanced  $\langle \text{weight} \rangle$  drives an overall enhancement in the total EEC  $A+A/p+p$  ratio in the small- $R_L$  region, while suppression of  $\langle \text{weight} \rangle$  further diminishes the enhancement of the paired-particle counts in the large- $R_L$  region.

#### IV. ATTRIBUTION AND SUMMARY

We have analyzed the differences in the  $A+A/p+p$   $R_L$  distributions between quark and gluon jets through four distinct dimensions: initial production mechanisms, variations in jet quenching mechanisms, internal substructure details revealed by EEC, and differential susceptibility to selection bias. We now investigate the fundamental origins of the flavor-dependent jet quenching effects observed in the EEC.



We therefore compute the A+A/p+p ratios of the EEC distributions under two counterfactual scenarios: pure gluon jets traversing the medium with quark-like energy loss characteristics, pure quark jets subjected to gluon-like energy loss dynamics. Results are presented in Fig. 9. These variations arise not only from differences in the interaction strength between quarks/gluons and the hot and dense medium, but also from distinct radiation patterns of gluons in radiative energy loss. We quantify this impact by highlighting the variation range between the nominal A+A/p+p ratio and our counterfactual ratio through shaded bands in the figure. For gluon jets with suppressed energy loss, we observe the expected attenuation of both energy loss and selection bias effects. However, enhancements persist across both small and large  $R_L$  regions. Conversely, enhancing quark energy loss to gluon-like levels dramatically amplifies the EEC distribution in A+A collisions at large  $R_L$  while preserving the characteristic suppression at small  $R_L$ .

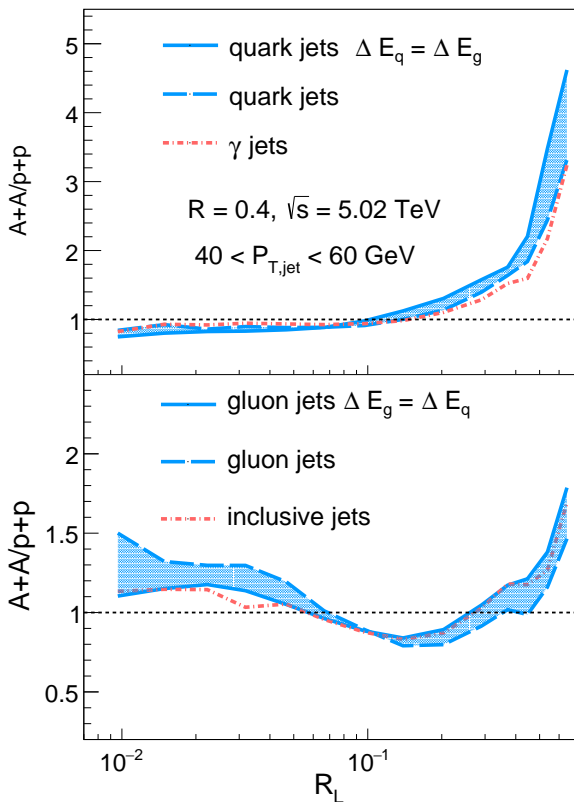


FIG. 9: Counterfactual analysis of flavor-dependent jet quenching via EEC distributions. (upper) Quark jets with energy loss equivalent to gluon jets ( $\Delta E_q = \Delta E_g$ ), compared to  $\gamma$ -tagged quark jets under standard quenching. (lower) Gluon jets with energy loss equivalent to quark jets ( $\Delta E_g = \Delta E_q$ ), compared to inclusive jets under standard quenching. All jets reconstructed with  $R = 0.4$  in central ( $0 - 10\%$ ) Pb+Pb collisions at  $\sqrt{s_{NN}} = 5.02$  TeV with transverse momentum  $40 < p_{T,jet} < 60$  GeV. Shaded bands indicate the variation range between nominal and counterfactual A+A/p+p ratios.

Consequently, the characteristic differences in A+A/p+p ratios of EEC distributions between quark- and gluon-initiated jets primarily stem from pre-quenching distribution disparities, not from flavor-dependent energy loss mechanisms, and crucially not from divergent gluon radiation patterns during radiative energy loss.

To experimentally observe and utilize this flavor-dependent difference, we propose photon-tagged jets as proxies for quark-initiated jets and inclusive charged-hadron jets within the same kinematic regime as proxies for gluon-initiated jets. We comparatively present the photon-tagged jets versus pure quark-initiated jets in the upper panel. The A+A/p+p ratios of EEC distributions for both jet types are compared within the same kinematic window. The photon-tagged jet results show notably closer alignment with unmodified quark-initiated jets. The inclusive charged-hadron jets are compared to pure gluon-initiated jets in the lower panel. The results for inclusive charged-hadron jets align closely with those of gluon-initiated jets, which have been artificially modified to undergo quark-like energy loss.

In summary, through PYTHIA simulations validated against ALICE p+p data and an improved SHELL model incorporating collisional/radiative energy loss plus medium response, we systematically quantify flavor-dependent jet quenching via energy-energy correlators (EEC) in  $\sqrt{s_{NN}} = 5.02$  TeV Pb+Pb collisions. Key findings include that the flavor-dependent quenching signatures in this study are characterized by pure quark jets exhibiting a strong enhancement at  $R_L > 0.2$ , and gluon jets displaying a bimodal enhancement at both small ( $R_L < 0.07$ ) and large ( $R_L > 0.4$ ) angular scales. Dual-shift decomposition is illustrated in the A+A/p+p ratio of the EEC, where shifts toward large  $R_L$  ( $> 0.3$ ) primarily stem from energy loss effects. Shifts toward small  $R_L$  ( $< 0.06$ ) are not fully attributable to selection bias. Counterfactual analysis reveals that intrinsic gluon jet enhancement is also evident in small- $R_L$  regions. The aspect of the substructure-resolved discrimination is that the quark jets suffer global suppression of  $\langle \text{weight} \rangle(R_L)$  and gluon jets suffer concentration of  $\langle \text{weight} \rangle$  toward small  $R_L$ . From the mechanism decomposition point of view, elastic energy loss concentrates  $\langle \text{weight} \rangle(R_L)$  toward small  $R_L$ , radiative energy loss dominates quark jet modifications, and medium response amplifies large  $R_L$  enhancement via soft hadron production. These results indicate that flavor dependence in EEC modifications is dominantly driven by intrinsic gluon/quark-initiated jet distribution structure differences rather than medium-induced mechanisms. At the end of the manuscript, we propose photon-tagged jets as proxies for quarks and inclusive charged-hadron jets as proxies for gluons.  $\gamma$ -tagged jets reproduce the pure quark jet quenching signatures, and inclusive jets exhibit gluon-like behavior when subjected to quark-like energy loss. These results establish the EEC as a precision probe of color-charge-dependent jet-medium interactions, providing new constraints for  $\hat{q}$  extraction and

QGP tomography. Meanwhile, the dominant role of initial jet structure suggests future analyses must account for pre-quenching flavor asymmetries.

**Acknowledgments:** This research is supported by

the Guangdong Major Project of Basic and Applied Basic Research No. 2020B0301030008, and the National Natural Science Foundation of China with Project Nos. 11935007 and 12035007. Ke-Ming Shen is supported by the Doctoral Research of ECUT (Nos. DHBK2019211).

- 
- [1] Miklos Gyulassy and Michael Plumer. Jet Quenching in Dense Matter. *Phys. Lett. B*, 243:432–438, 1990.
  - [2] Xiaofeng Luo and Nu Xu. Search for the QCD Critical Point with Fluctuations of Conserved Quantities in Relativistic Heavy-Ion Collisions at RHIC : An Overview. *Nucl. Sci. Tech.*, 28(8):112, 2017.
  - [3] Zebo Tang, Ze-Bo Tang, Wangmei Zha, Wang-Mei Zha, Yifei Zhang, and Yi-Fei Zhang. An experimental review of open heavy flavor and quarkonium production at RHIC. *Nucl. Sci. Tech.*, 31(8):81, 2020.
  - [4] He-Xia Zhang, Yu-Xin Xiao, Jin-Wen Kang, and Ben-Wei Zhang. Phenomenological study of the anisotropic quark matter in the two-flavor Nambu–Jona–Lasinio model. *Nucl. Sci. Tech.*, 33(11):150, 2022.
  - [5] Qi-Ye Shou et al. Properties of QCD matter: a review of selected results from ALICE experiment. *Nucl. Sci. Tech.*, 35(12):219, 2024.
  - [6] Xin-Nian Wang and Miklos Gyulassy. Gluon shadowing and jet quenching in A + A collisions at  $s^{*}(1/2) = 200$ -GeV. *Phys. Rev. Lett.*, 68:1480–1483, 1992.
  - [7] Miklos Gyulassy, Ivan Vitev, Xin-Nian Wang, and Ben-Wei Zhang. Jet quenching and radiative energy loss in dense nuclear matter. pages 123–191, 2004.
  - [8] Guang-You Qin and Xin-Nian Wang. Jet quenching in high-energy heavy-ion collisions. *Int. J. Mod. Phys. E*, 24(11):1530014, 2015.
  - [9] Clint Young, Bjorn Schenke, Sangyong Jeon, and Charles Gale. Dijet asymmetry at the energies available at the CERN Large Hadron Collider. *Phys. Rev. C*, 84:024907, 2011.
  - [10] Yuncun He, Ivan Vitev, and Ben-Wei Zhang.  $\mathcal{O}(\alpha_s^3)$  Analysis of Inclusive Jet and di-Jet Production in Heavy Ion Reactions at the Large Hadron Collider. *Phys. Lett. B*, 713:224–232, 2012.
  - [11] R. B. Neufeld, I. Vitev, and B. W. Zhang. The Physics of  $Z^0/\gamma^*$ -tagged jets at the LHC. *Phys. Rev. C*, 83:034902, 2011.
  - [12] Korinna C. Zapp, Frank Krauss, and Urs A. Wiedemann. A perturbative framework for jet quenching. *JHEP*, 03:080, 2013.
  - [13] Wei Dai, Ivan Vitev, and Ben-Wei Zhang. Momentum imbalance of isolated photon-tagged jet production at RHIC and LHC. *Phys. Rev. Lett.*, 110(14):142001, 2013.
  - [14] Guo-Liang Ma. Dijet asymmetry in Pb+Pb collisions at  $\sqrt{s_{NN}}=2.76$  TeV within a multiphase transport model. *Phys. Rev. C*, 87(6):064901, 2013.
  - [15] Florian Senzel, Oliver Fochler, Jan Uphoff, Zhe Xu, and Carsten Greiner. Influence of multiple in-medium scattering processes on the momentum imbalance of reconstructed di-jets. *J. Phys. G*, 42(11):115104, 2015.
  - [16] Jorge Casalderrey-Solana, Doga Can Gulhan, José Guilherme Milhano, Daniel Pablos, and Krishna Rajagopal. A Hybrid Strong/Weak Coupling Approach to Jet Quenching. *JHEP*, 10:019, 2014. [Erratum: JHEP 09, 175 (2015)].
  - [17] José Guilherme Milhano and Korinna Christine Zapp. Origins of the di-jet asymmetry in heavy ion collisions. *Eur. Phys. J. C*, 76(5):288, 2016.
  - [18] Ning-Bo Chang and Guang-You Qin. Full jet evolution in quark-gluon plasma and nuclear modification of jet production and jet shape in Pb+Pb collisions at 2.76A TeV at the CERN Large Hadron Collider. *Phys. Rev. C*, 94(2):024902, 2016.
  - [19] A. Majumder and J. Putschke. Mass depletion: a new parameter for quantitative jet modification. *Phys. Rev. C*, 93(5):054909, 2016.
  - [20] Lin Chen, Guang-You Qin, Shu-Yi Wei, Bo-Wen Xiao, and Han-Zhong Zhang. Dijet Asymmetry in the Resummation Improved Perturbative QCD Approach. *Phys. Lett. B*, 782:773–778, 2018.
  - [21] Yang-Ting Chien and Ivan Vitev. Probing the Hardest Branching within Jets in Heavy-Ion Collisions. *Phys. Rev. Lett.*, 119(11):112301, 2017.
  - [22] Liliana Apolinário, José Guilherme Milhano, Mateusz Ploskon, and Xiaoming Zhang. Novel subjet observables for jet quenching in heavy-ion collisions. *Eur. Phys. J. C*, 78(6):529, 2018.
  - [23] Megan Connors, Christine Nattrass, Rosi Reed, and Sevil Salur. Jet measurements in heavy ion physics. *Rev. Mod. Phys.*, 90:025005, 2018.
  - [24] Shan-Liang Zhang, Tan Luo, Xin-Nian Wang, and Ben-Wei Zhang. Z+jet correlation with NLO-matched parton-shower and jet-medium interaction in high-energy nuclear collisions. *Phys. Rev. C*, 98:021901, 2018.
  - [25] Wei Dai, Sa Wang, Shan-Liang Zhang, Ben-Wei Zhang, and Enke Wang. Transverse Momentum Balance and Angular Distribution of  $b\bar{b}$  Dijets in Pb+Pb collisions. *Chin. Phys. C*, 44:104105, 2020.
  - [26] Tan Luo, Shanshan Cao, Yayun He, and Xin-Nian Wang. Multiple jets and  $\gamma$ -jet correlation in high-energy heavy-ion collisions. *Phys. Lett. B*, 782:707–716, 2018.
  - [27] Ning-Bo Chang, Yasuki Tachibana, and Guang-You Qin. Nuclear modification of jet shape for inclusive jets and  $\gamma$ -jets at the LHC energies. *Phys. Lett. B*, 801:135181, 2020.
  - [28] Sa Wang, Wei Dai, Ben-Wei Zhang, and Enke Wang. Diffusion of charm quarks in jets in high-energy heavy-ion collisions. *Eur. Phys. J. C*, 79(9):789, 2019.
  - [29] Shi-Yong Chen, Ben-Wei Zhang, and En-Ke Wang. Jet charge in high energy nuclear collisions. *Chin. Phys. C*, 44(2):024103, 2020.
  - [30] Lin Chen, Shu-Yi Wei, and Han-Zhong Zhang. Probing jet medium interactions via  $Z(H) + \text{jet}$  momentum imbalances. *Eur. Phys. J. C*, 80(12):1136, 2020.
  - [31] Sa Wang, Wei Dai, Ben-Wei Zhang, and Enke Wang.  $Z^0$  boson associated b-jet production in high-energy nuclear collisions\*. *Chin. Phys. C*, 47(5):054102, 2023.
  - [32] Jun Yan, Shi-Yong Chen, Wei Dai, Ben-Wei Zhang, and Enke Wang. Medium modifications of girth distributions for inclusive jets and  $Z^0 + \text{jet}$  in relativistic heavy-ion collisions at the LHC. *Chin. Phys. C*, 45(2):024102, 2021.

- [33] Sa Wang, Wei Dai, Ben-Wei Zhang, and Enke Wang. Radial profile of bottom quarks in jets in high-energy nuclear collisions. *Chin. Phys. C*, 45(6):064105, 2021.
- [34] Shan-Liang Zhang, Meng-Quan Yang, and Ben-Wei Zhang. Parton splitting scales of reclustered large-radius jets in high-energy nuclear collisions. *Eur. Phys. J. C*, 82(5):414, 2022.
- [35] Yao Li, Shuwan Shen, Sa Wang, and Ben-Wei Zhang. Transverse momentum balance of dijets in Xe+Xe collisions at the LHC. *Nucl. Sci. Tech.*, 35(7):113, 2024.
- [36] Yang-Ting Chien and Ivan Vitev. Towards the understanding of jet shapes and cross sections in heavy ion collisions using soft-collinear effective theory. *JHEP*, 05:023, 2016.
- [37] Albert M Sirunyan et al. Jet Shapes of Isolated Photon-Tagged Jets in Pb-Pb and pp Collisions at  $\sqrt{s_{NN}} = 5.02$  TeV. *Phys. Rev. Lett.*, 122(15):152001, 2019.
- [38] Zhong Yang, Tan Luo, Wei Chen, Long-Gang Pang, and Xin-Nian Wang. 3D Structure of Jet-Induced Diffusion Wake in an Expanding Quark-Gluon Plasma. *Phys. Rev. Lett.*, 130(5):052301, 2023.
- [39] Jorge Casalderrey-Solana, Doga Gulhan, Guilherme Milhano, Daniel Pablos, and Krishna Rajagopal. Angular Structure of Jet Quenching Within a Hybrid Strong/Weak Coupling Model. *JHEP*, 03:135, 2017.
- [40] Albert M Sirunyan et al. Observation of Medium-Induced Modifications of Jet Fragmentation in Pb-Pb Collisions at  $\sqrt{s_{NN}} = 5.02$  TeV Using Isolated Photon-Tagged Jets. *Phys. Rev. Lett.*, 121(24):242301, 2018.
- [41] Morad Aaboud et al. Measurement of jet fragmentation in Pb+Pb and *pp* collisions at  $\sqrt{s_{NN}} = 5.02$  TeV with the ATLAS detector. *Phys. Rev. C*, 98(2):024908, 2018.
- [42] Wei Chen, Shanshan Cao, Tan Luo, Long-Gang Pang, and Xin-Nian Wang. Medium modification of  $\gamma$ -jet fragmentation functions in Pb+Pb collisions at LHC. *Phys. Lett. B*, 810:135783, 2020.
- [43] Shreyasi Acharya et al. Measurement of the groomed jet radius and momentum splitting fraction in pp and Pb-Pb collisions at  $\sqrt{s_{NN}} = 5.02$  TeV. *Phys. Rev. Lett.*, 128(10):102001, 2022.
- [44] C. Louis Basham, Lowell S. Brown, S. D. Ellis, and S. T. Love. Electron - Positron Annihilation Energy Pattern in Quantum Chromodynamics: Asymptotically Free Perturbation Theory. *Phys. Rev. D*, 17:2298, 1978.
- [45] C. Louis Basham, Lowell S. Brown, Stephen D. Ellis, and Sherwin T. Love. Energy Correlations in electron - Positron Annihilation: Testing QCD. *Phys. Rev. Lett.*, 41:1585, 1978.
- [46] C. L. Basham, L. S. Brown, S. D. Ellis, and S. T. Love. Energy Correlations in electron-Positron Annihilation in Quantum Chromodynamics: Asymptotically Free Perturbation Theory. *Phys. Rev. D*, 19:2018, 1979.
- [47] Christoph Berger et al. A Study of Energy-energy Correlations in  $e^+e^-$  Annihilations at  $\sqrt{s} = 34.6$ -GeV. *Z. Phys. C*, 28:365, 1985.
- [48] Andrew J. Larkoski, Gavin P. Salam, and Jesse Thaler. Energy Correlation Functions for Jet Substructure. *JHEP*, 06:108, 2013.
- [49] Andrew J. Larkoski and Ian Moult. The Singular Behavior of Jet Substructure Observables. *Phys. Rev. D*, 93:014017, 2016.
- [50] Lance J. Dixon, Ming-Xing Luo, Vladyslav Shtabovenko, Tong-Zhi Yang, and Hua Xing Zhu. Analytical Computation of Energy-Energy Correlation at Next-to-Leading Order in QCD. *Phys. Rev. Lett.*, 120(10):102001, 2018.
- [51] Hao Chen, Ming-Xing Luo, Ian Moult, Tong-Zhi Yang, Xiaoyuan Zhang, and Hua Xing Zhu. Three point energy correlators in the collinear limit: symmetries, dualities and analytic results. *JHEP*, 08(08):028, 2020.
- [52] J. M. Henn, E. Sokatchev, K. Yan, and A. Zhiboedov. Energy-energy correlation in  $N=4$  super Yang-Mills theory at next-to-next-to-leading order. *Phys. Rev. D*, 100(3):036010, 2019.
- [53] Hao Chen, Ian Moult, Xiaoyuan Zhang, and Hua Xing Zhu. Rethinking jets with energy correlators: Tracks, resummation, and analytic continuation. *Phys. Rev. D*, 102(5):054012, 2020.
- [54] Jun Gao, Vladyslav Shtabovenko, and Tong-Zhi Yang. Energy-energy correlation in hadronic Higgs decays: analytic results and phenomenology at NLO. *JHEP*, 02:210, 2021.
- [55] Hai Tao Li, Yiannis Makris, and Ivan Vitev. Energy-energy correlators in Deep Inelastic Scattering. *Phys. Rev. D*, 103(9):094005, 2021.
- [56] Patrick T. Komiske, Ian Moult, Jesse Thaler, and Hua Xing Zhu. Analyzing N-Point Energy Correlators inside Jets with CMS Open Data. *Phys. Rev. Lett.*, 130(5):051901, 2023.
- [57] Duff Neill, Gherardo Vita, Ivan Vitev, and Hua Xing Zhu. Energy-Energy Correlators for Precision QCD. In *Snowmass 2021*, 3 2022.
- [58] Xiaohui Liu and Hua Xing Zhu. Nucleon Energy Correlators. *Phys. Rev. Lett.*, 130(9):091901, 2023.
- [59] Hao Chen, Ian Moult, Jesse Thaler, and Hua Xing Zhu. Non-Gaussianities in collider energy flux. *JHEP*, 07:146, 2022.
- [60] Jack Holguin, Ian Moult, Aditya Pathak, and Massimiliano Procura. New paradigm for precision top physics: Weighing the top with energy correlators. *Phys. Rev. D*, 107(11):114002, 2023.
- [61] Kyle Lee, Bianka Meçaj, and Ian Moult. Conformal collider physics meets LHC data. *Phys. Rev. D*, 111(1):L011502, 2025.
- [62] Hao-Yu Liu, Xiaohui Liu, Ji-Chen Pan, Feng Yuan, and Hua Xing Zhu. Nucleon Energy Correlators for the Color Glass Condensate. *Phys. Rev. Lett.*, 130(18):181901, 2023.
- [63] Haotian Cao, Xiaohui Liu, and Hua Xing Zhu. Toward precision measurements of nucleon energy correlators in lepton-nucleon collisions. *Phys. Rev. D*, 107(11):114008, 2023.
- [64] Wen Chen, Jun Gao, Yibei Li, Zhen Xu, Xiaoyuan Zhang, and Hua Xing Zhu. NNLL resummation for projected three-point energy correlator. *JHEP*, 05:043, 2024.
- [65] Max Jaarsma, Yibei Li, Ian Moult, Wouter J. Waalewijn, and Hua Xing Zhu. Energy correlators on tracks: resummation and non-perturbative effects. *JHEP*, 12:087, 2023.
- [66] Kyle Lee and Ian Moult. Energy Correlators Taking Charge. 8 2023.
- [67] Zhong-Bo Kang, Kyle Lee, Ding Yu Shao, and Fanyi Zhao. Probing transverse momentum dependent structures with azimuthal dependence of energy correlators. *JHEP*, 03:153, 2024.
- [68] Zhong-Bo Kang, Kyle Lee, Ding Yu Shao, and Fanyi Zhao. Collins-type Energy-Energy Correlators and Nucleon Structure. In *30th International Workshop on Deep-Inelastic Scattering and Related Subjects*, 7 2023.

- [69] An-Ping Chen, Xiaohui Liu, and Yan-Qing Ma. Shedding Light on Hadronization by Quarkonium Energy Correlator. *Phys. Rev. Lett.*, 133:19, 2024.
- [70] João Barata, José Guilherme Milhano, and Andrey V. Sadofyev. Picturing QCD jets in anisotropic matter: from jet shapes to energy energy correlators. *Eur. Phys. J. C*, 84(2):174, 2024.
- [71] Jack Holguin, Ian Moulton, Aditya Pathak, Massimiliano Procura, Robert Schöfbeck, and Dennis Schwarz. Using the W Boson as a Standard Candle to Reach the Top: Calibrating Energy-Correlator-Based Top Mass Measurements. *Phys. Rev. Lett.*, 134(23):231903, 2025.
- [72] João Barata and Robert Szafron. Leading order track functions in a hot and dense QGP. *Phys. Rev. D*, 110(3):L031501, 2024.
- [73] Samuel Alipour-fard and Wouter J. Waalewijn. Energy Correlators Beyond Angles. 1 2025.
- [74] Evan Craft, Kyle Lee, Bianka Meçaj, and Ian Moulton. Beautiful and Charming Energy Correlators. 10 2022.
- [75] Carlota Andres, Fabio Dominguez, Raghav Kunawalkam Elayavalli, Jack Holguin, Cyrille Marquet, and Ian Moulton. Resolving the Scales of the Quark-Gluon Plasma with Energy Correlators. *Phys. Rev. Lett.*, 130(26):262301, 2023.
- [76] Carlota Andres, Fabio Dominguez, Jack Holguin, Cyrille Marquet, and Ian Moulton. A coherent view of the quark-gluon plasma from energy correlators. *JHEP*, 09:088, 2023.
- [77] João Barata and Yacine Mehtar-Tani. Energy loss effects in EECs at LO. *PoS, HardProbes2023*:145, 2024.
- [78] João Barata, Paul Caucal, Alba Soto-Ontoso, and Robert Szafron. Advancing the understanding of energy-energy correlators in heavy-ion collisions. *JHEP*, 11:060, 2024.
- [79] Balbeer Singh and Varun Vaidya. Factorization for energy-energy correlator in heavy ion collision. *JHEP*, 06:071, 2025.
- [80] Carlota Andres, Fabio Dominguez, Jack Holguin, Cyrille Marquet, and Ian Moulton. Seeing beauty in the quark-gluon plasma with energy correlators. *Phys. Rev. D*, 110(3):L031503, 2024.
- [81] Carlota Andres, Fabio Dominguez, Jack Holguin, Cyrille Marquet, and Ian Moulton. Simple Scaling Laws for Energy Correlators in Nuclear Matter. 11 2024.
- [82] Carlota Andres, Fabio Dominguez, Jack Holguin, Cyrille Marquet, and Ian Moulton. Towards an interpretation of the first measurements of energy correlators in the quark-gluon plasma. *JHEP*, 03:166, 2025.
- [83] Zhong Yang, Yayun He, Ian Moulton, and Xin-Nian Wang. Probing the Short-Distance Structure of the Quark-Gluon Plasma with Energy Correlators. *Phys. Rev. Lett.*, 132(1):011901, 2024.
- [84] Hannah Bossi, Arjun Srinivasan Kudinoor, Ian Moulton, Daniel Pablos, Ananya Rai, and Krishna Rajagopal. Imaging the wakes of jets with energy-energy-energy correlators. *JHEP*, 12:073, 2024.
- [85] Wen-Jing Xing, Shanshan Cao, Guang-You Qin, and Xin-Nian Wang. Flavor Hierarchy of Jet Energy Correlators inside the Quark-Gluon Plasma. *Phys. Rev. Lett.*, 134(5):052301, 2025.
- [86] João Barata, Matvey V. Kuzmin, José Guilherme Milhano, and Andrey V. Sadofyev. Jet EEC aWAKENing: hydrodynamic response on the celestial sphere. 12 2024.
- [87] Kyle Devereaux, Wenqing Fan, Weiyao Ke, Kyle Lee, and Ian Moulton. Imaging Cold Nuclear Matter with Energy Correlators. 3 2023.
- [88] Yu Fu, Berndt Müller, and Chathuranga Sirimanna. Modification of the Jet Energy-Energy Correlator in Cold Nuclear Matter. 11 2024.
- [89] João Barata, Zhong-Bo Kang, Xoán Mayo López, and Jani Penttala. Energy-Energy Correlator for jet production in  $pp$  and  $pA$  collisions. 11 2024.
- [90] Carlota Andres, Jack Holguin, Raghav Kunawalkam Elayavalli, and Jussi Viinikainen. Minimizing Selection Bias in Inclusive Jets in Heavy-Ion Collisions with Energy Correlators. *Phys. Rev. Lett.*, 134(8):082303, 2025.
- [91] Carlota Andres and Jack Holguin. Minimizing Selection Bias in Inclusive Jets in Heavy-Ion Collisions with Energy Correlators – arXiv note. 9 2024.
- [92] Andrew Tamis. Measurement of Two-Point Energy Correlators Within1 Jets in  $p p$  Collisions at  $\sqrt{s} = 200$  GeV at STAR. *PoS, HardProbes2023*:175, 2024.
- [93] Energy-energy correlators from PbPb and pp collisions at 5.02 TeV. 2024.
- [94] Shreyasi Acharya et al. Exposing the parton-hadron transition within jets with energy-energy correlators in pp collisions at  $\sqrt{s} = 5.02$  TeV. 9 2024.
- [95] Shreyasi Acharya et al. Energy-energy correlators in charm-tagged jets in proton-proton collisions at  $\sqrt{s} = 13$  TeV. 4 2025.
- [96] Xin-Nian Wang. Effect of jet quenching on high  $p_T$  hadron spectra in high-energy nuclear collisions. *Phys. Rev. C*, 58:2321, 1998.
- [97] R. Baier, Yuri L. Dokshitzer, Alfred H. Mueller, S. Peigne, and D. Schiff. Radiative energy loss and  $p(T)$  broadening of high-energy partons in nuclei. *Nucl. Phys. B*, 484:265–282, 1997.
- [98] Xin-Nian Wang and Xiao-feng Guo. Multiple parton scattering in nuclei: Parton energy loss. *Nucl. Phys. A*, 696:788–832, 2001.
- [99] Peter Brockway Arnold, Guy D. Moore, and Laurence G. Yaffe. Transport coefficients in high temperature gauge theories. 1. Leading log results. *JHEP*, 11:001, 2000.
- [100] M. Gyulassy, P. Levai, and I. Vitev. Reaction operator approach to nonAbelian energy loss. *Nucl. Phys. B*, 594:371–419, 2001.
- [101] Hai Tao Li and Ivan Vitev. Jet charge modification in dense QCD matter. *Phys. Rev. D*, 101:076020, 2020.
- [102] Albert M Sirunyan et al. Measurement of quark- and gluon-like jet fractions using jet charge in PbPb and pp collisions at 5.02 TeV. *JHEP*, 07:115, 2020.
- [103] Yang-Ting Chien and Raghav Kunawalkam Elayavalli. Probing heavy ion collisions using quark and gluon jet substructure. 3 2018.
- [104] Torbjörn Sjöstrand, Stefan Ask, Jesper R. Christiansen, Richard Corke, Nishita Desai, Philip Ilten, Stephen Mrenna, Stefan Prestel, Christine O. Rasmussen, and Peter Z. Skands. An introduction to PYTHIA 8.2. *Comput. Phys. Commun.*, 191:159–177, 2015.
- [105] Peter Skands, Stefano Carrazza, and Juan Rojo. Tuning PYTHIA 8.1: the Monash 2013 Tune. *Eur. Phys. J. C*, 74(8):3024, 2014.
- [106] Matteo Cacciari, Gavin P. Salam, and Gregory Soyez. The anti- $k_t$  jet clustering algorithm. *JHEP*, 04:063, 2008.
- [107] Shi-Yong Chen, Jun Yan, Wei Dai, Ben-Wei Zhang, and Enke Wang.  $p_T$  dispersion of inclusive jets in high-energy nuclear collisions\*. *Chin. Phys. C*,

- 46(10):104102, 2022.
- [108] Wei Dai, Ming-Ze Li, Ben-Wei Zhang, and Enke Wang. Exposing the dead-cone effect of jet quenching in QCD medium. 5 2022.
  - [109] Yao Li, Sa Wang, and Ben-Wei Zhang. Longitudinal momentum fraction of heavy-flavor mesons in jets in high-energy nuclear collisions. *Phys. Rev. C*, 108(2):024905, 2023.
  - [110] Sa Wang, Yao Li, Jin-Wen Kang, and Ben-Wei Zhang. Unveiling the jet angular broadening with  $\gamma$ -jet in high-energy nuclear collisions. 8 2024.
  - [111] Yao Li, Shi-Yong Chen, Weixi Kong, Sa Wang, and Ben-Wei Zhang. Medium modifications of heavy-flavor jet angularities in high-energy nuclear collisions. 9 2024.
  - [112] B. Alver, M. Baker, C. Loizides, and P. Steinberg. The PHOBOS Glauber Monte Carlo. 5 2008.
  - [113] Abhijit Majumder. Hard collinear gluon radiation and multiple scattering in a medium. *Phys. Rev. D*, 85:014023, 2012.
  - [114] Xiao-feng Guo and Xin-Nian Wang. Multiple scattering, parton energy loss and modified fragmentation functions in deeply inelastic e A scattering. *Phys. Rev. Lett.*, 85:3591–3594, 2000.
  - [115] Ben-Wei Zhang and Xin-Nian Wang. Multiple parton scattering in nuclei: Beyond helicity amplitude approximation. *Nucl. Phys. A*, 720:429–451, 2003.
  - [116] Shanshan Cao, Tan Luo, Guang-You Qin, and Xin-Nian Wang. Heavy and light flavor jet quenching at RHIC and LHC energies. *Phys. Lett. B*, 777:255–259, 2018.
  - [117] R. B. Neufeld. Thermal field theory derivation of the source term induced by a fast parton from the quark energy-momentum tensor. *Phys. Rev. D*, 83:065012, 2011.
  - [118] Chun Shen, Zhi Qiu, Huichao Song, Jonah Bernhard, Steffen Bass, and Ulrich Heinz. The iEBE-VISHNU code package for relativistic heavy-ion collisions. *Comput. Phys. Commun.*, 199:61–85, 2016.
  - [119] J. H. Putschke et al. The JETSCAPE framework. 3 2019.
  - [120] Fred Cooper and Graham Frye. Comment on the Single Particle Distribution in the Hydrodynamic and Statistical Thermodynamic Models of Multiparticle Production. *Phys. Rev. D*, 10:186, 1974.